

Hawking Radiation Spectra for Scalar Fields by a Higher-Dimensional Schwarzschild-de-Sitter Black Hole

T. Pappas¹, P. Kanti¹ and N. Pappas²

¹*Division of Theoretical Physics, Department of Physics,
University of Ioannina, Ioannina GR-45110, Greece*

²*Nuclear and Particle Physics Section, Physics Department,
National and Kapodistrian University of Athens, Athens GR-15771, Greece*

Abstract

In this work, we study the propagation of scalar fields in the gravitational background of a higher-dimensional Schwarzschild-de-Sitter black hole as well as on the projected-on-the-brane 4-dimensional background. The scalar fields have also a non-minimal coupling to the corresponding, bulk or brane, scalar curvature. We perform a comprehensive study by deriving exact numerical results for the greybody factors, and study their profile in terms of particle and spacetime properties. We then proceed to derive the Hawking radiation spectra for a higher-dimensional Schwarzschild-de-Sitter black hole, and we study both bulk and brane channels. We demonstrate that the non-minimal field coupling, that creates an effective mass term for the fields, suppresses the energy emission rates while the cosmological constant assumes a dual role. By computing the relative energy rates and the total emissivity ratio for bulk and brane emission, we demonstrate that the combined effect of a large number of extra dimensions and value of the field coupling gives to the bulk channel the clear domination in the bulk-brane energy balance.

1 Introduction

Black holes in four dimensions have been studied in the context of General Theory of Relativity, with their spacetime properties and existence criteria being classified in detail. In the context, however, of the theories with extra spacelike dimensions [1, 2] that were proposed more than fifteen years ago, all the above have been re-considered. In fact, the first gravitational solution describing a higher-dimensional, spherically-symmetric black hole formed in the presence of a cosmological constant was found many decades before the formulation of the aforementioned theories, and is known as the higher-dimensional Schwarzschild-de-Sitter or Tangherlini solution [3].

One of the features that have always attracted the interest of scientists is the emission of Hawking radiation [4] by black holes: it is the manifestation of a quantum effect in a curved spacetime, that unfortunately has never been detected so far in the universe. The idea of the existence of extra spacelike dimensions has given a boost also to this direction, since extra dimensions may facilitate the creation of mini black holes at particle colliders and thus the observation of the associated Hawking radiation. As a result, the derivation of the Hawking radiation spectra from higher-dimensional black holes has been the topic of a significant number of works - for a partial list see [5]-[23] while for a more extensive set of references one may consult the reviews [24]-[34].

There have been rather few attempts to determine the form and features of the Hawking radiation emission spectra for a higher-dimensional Schwarzschild-de-Sitter black hole. The first such work appeared in 2005 [35], and provided exact numerical results for minimally-coupled scalar fields propagating both on the brane and in the bulk and an analytic study for the lowest partial mode and at the low-energy regime. Soon afterwards, another analytic study [36] determined the next-to-leading-order term in the expansion of the greybody factor in terms of the energy of the scalar particle, again for the lowest partial mode. In 2008, another numerical study [37] addressed the question of the emission of fields with arbitrary spin from a higher-dimensional Schwarzschild-de-Sitter black hole.

A much more recent study [38], that appeared in 2013, raised the possibility that the scalar field has also a non-minimal coupling with the scalar curvature, and provided an analytic formulation of the greybody factor for all partial modes. However, as this analysis was restricted in the case of a 4-dimensional Schwarzschild-de-Sitter black hole, a work of the present authors [39] appeared a year later containing an analytic study of the higher-dimensional case that provided analytic expressions for the greybody factors for propagation of non-minimally coupled scalar fields both in the bulk and on the brane. The properties of the greybody factors in terms of the particle and spacetime parameters were studied in detail, however, the validity of the analysis was limited due to the necessary assumption that both the value of the cosmological constant and the non-minimal coupling constant had to be small. Recently, two additional works appeared [40, 41] that focused again on the analytic, low-energy derivation of greybody factors for fields propagating in the background of a Schwarzschild-de-Sitter black hole.

The aforementioned restriction to the values of the parameters of the model, involved always in the analytic studies, cannot allow the derivation of the complete Hawking radi-

ation spectra that need the exact form of the greybody factors valid for arbitrary values of the parameters. To this end, we return to the study of non-minimally coupled scalar fields propagating in the background of a higher-dimensional Schwarzschild-de-Sitter black hole, in order to derive the exact values of the greybody factors for fields propagating both in the bulk and on the brane. We will study each case separately, assume in general a non-vanishing coupling of the field with the corresponding scalar curvature, and solve by numerical integration the radial part of the field equation, in terms of which we may determine the greybody factor. Our previously found analytic solutions will serve as asymptotic boundary conditions for our numerical analysis. We will compare the numerical results for the greybody factors with the previously found analytic ones, and then we will study their profile in terms of the particle parameters (angular-momentum number and non-minimal coupling constant) and spacetime properties (number of extra dimensions and value of cosmological constant).

Next, we will proceed to derive the differential energy emission rates for Hawking radiation from a higher-dimensional Schwarzschild-de-Sitter black hole in the form of scalar fields, both in the bulk and on the brane. Again, the profile of the emission curves in terms of the parameters of the model will be studied in a comprehensive way. Having the complete power spectra at our disposal, we will also compute the relative energy rates for bulk and brane emission as well as the total emissivity ratio between the two channels. The amount of the energy of the black hole that is emitted on our brane, where the 4-dimensional potential observer lives, has always been an important one; therefore, in the context of this work also, we will attempt to determine whether the brane domination still persists or whether it is affected, and maybe overthrown, by factors of this model.

The outline of our paper is as follows: in Section 2, we present the theoretical framework of our analysis, the gravitational background, and the equations of motion for the propagation of the scalar fields both in the bulk and on the brane. In Section 3, we focus on the derivation of the greybody factors for brane and bulk scalar fields by numerically solving the corresponding radial equations. In Section 4, we determine the differential energy emission rates, for both types of scalar fields again, study their profile and finally address the question of the relative emission rates and the total emissivity ratio. We present our conclusions in Section 5.

2 The Theoretical Framework

Let us start by determining first the gravitational background for our analysis. We will consider the following higher-dimensional gravitational theory

$$S_D = \int d^{4+n}x \sqrt{-G} \left(\frac{R_D}{2\kappa_D^2} - \Lambda \right), \quad (1)$$

where $D = 4+n$ is the dimensionality of spacetime, with n denoting an arbitrary number of space-like dimensions. Also, $\kappa_D^2 = 1/M_*^{2+n}$ is the higher-dimensional gravitational constant, with M_* being the fundamental scale of gravity, and R_D the higher-dimensional Ricci scalar. Finally, G stands for the determinant of the metric tensor G_{MN} and Λ is a positive bulk cosmological constant.

If we vary the above action with respect to the metric tensor G_{MN} , we obtain the Einstein's field equations that have the form

$$R_{MN} - \frac{1}{2} G_{MN} R_D = -\kappa_D^2 G_{MN} \Lambda. \quad (2)$$

The above set of equations admit a spherically-symmetric $(4+n)$ -dimensional solution, known as the Tangherlini solution [3], of the form

$$ds^2 = -h(r) dt^2 + \frac{dr^2}{h(r)} + r^2 d\Omega_{2+n}^2, \quad (3)$$

where

$$h(r) = 1 - \frac{\mu}{r^{n+1}} - \frac{2\kappa_D^2 \Lambda r^2}{(n+3)(n+2)}, \quad (4)$$

and $d\Omega_{2+n}^2$ is the area of the $(2+n)$ -dimensional unit sphere given by

$$d\Omega_{2+n}^2 = d\theta_{n+1}^2 + \sin^2 \theta_{n+1} \left(d\theta_n^2 + \sin^2 \theta_n \left(\dots + \sin^2 \theta_2 (d\theta_1^2 + \sin^2 \theta_1 d\varphi^2) \dots \right) \right). \quad (5)$$

The above solution describes a higher-dimensional Schwarzschild-de-Sitter spacetime, with the parameter μ associated with the black-hole mass M through the relation [42]

$$\mu = \frac{\kappa_D^2 M}{(n+2)} \frac{\Gamma[(n+3)/2]}{\pi^{(n+3)/2}}. \quad (6)$$

Depending on the values of the parameters M and Λ , the Schwarzschild-de-Sitter spacetime may have two, one or zero horizons [43], that correspond to the real, positive roots of the equation $h(r) = 0$. Throughout our analysis, we will assume that the values of those parameters are such so that the spacetime has always two horizons: these will be the black-hole horizon, at $r = r_h$, and the cosmological horizon, at $r = r_c$; the region of interest will be the area in between, i.e. $r_h < r < r_c$.

We will now assume that a scalar field propagates in the aforementioned Schwarzschild-de-Sitter spacetime (3). This field may couple to gravity either minimally or non-minimally and, accordingly, it will be described by the action

$$S_\Phi = -\frac{1}{2} \int d^{4+n}x \sqrt{-G} [\xi \Phi^2 R_D + \partial_M \Phi \partial^M \Phi]. \quad (7)$$

In the above, ξ is a positive, constant coupling function: for $\xi = 0$, we obtain the case of minimal coupling, while for $\xi \neq 0$, the scalar field couples to the higher-dimensional Ricci scalar. The latter quantity may easily be found by contracting the Einstein's field equations (2) by the inverse metric tensor G^{MN} and is given by the expression

$$R_D = \frac{2(n+4)}{n+2} \kappa_D^2 \Lambda. \quad (8)$$

We note that R_D is determined by the bulk cosmological constant as expected, however, it also carries a dependence on the number of extra spacelike dimensions exhibiting a slight decrease as n increases.

The variation of S_Φ with respect to the scalar field leads to its equation of motion that reads

$$\frac{1}{\sqrt{-G}} \partial_M \left(\sqrt{-G} G^{MN} \partial_N \Phi \right) = \xi R_D \Phi. \quad (9)$$

As is usual, we will assume that the effect of the propagation of this massless scalar field on the spacetime background is negligible, and thus Eq. (9) will be solved for a fixed background given by (3). To this end, we assume a factorized ansatz for the scalar field of the form

$$\Phi(t, r, \theta_i, \varphi) = e^{-i\omega t} R(r) \tilde{Y}(\theta_i, \varphi), \quad (10)$$

where $\tilde{Y}(\theta_i, \varphi)$ are the hyperspherical harmonics [44]. By using the eigenvalue equation of the latter, we may easily decouple the radial part of Eq. (9) from its angular part ending up with the radial equation [39]

$$\frac{1}{r^{n+2}} \frac{d}{dr} \left(h r^{n+2} \frac{dR}{dr} \right) + \left[\frac{\omega^2}{h} - \frac{l(l+n+1)}{r^2} - \xi R_D \right] R = 0. \quad (11)$$

In [39], Eq. (11) was also written in the form of a Schrödinger-like equation with the effective potential ‘felt’ by the bulk scalar field having the explicit form

$$V_{\text{eff}}^{\text{bulk}} = h(r) \left\{ \frac{(2l+n+1)^2 - 1}{4r^2} + \kappa_D^2 \Lambda (n+4) \left[\frac{2\xi}{(n+2)} - \frac{1}{2(n+3)} \right] + \frac{(n+2)^2 \mu}{4r^{n+3}} \right\}. \quad (12)$$

The potential bears a dependence on both spacetime and particle properties. Its detailed study in [39] revealed that it has the form of a barrier whose height increases with the number of extra dimensions n of spacetime as well as with the angular-momentum number l and coupling parameter ξ of the scalar field. The profile of the potential in terms of the bulk cosmological constant is more subtle: the height of the barrier decreases with Λ for vanishing or small values of ξ , but it increases for large values of ξ . Independently of the values of the aforementioned parameters, the effective potential always vanishes at the location of the two horizons, r_h and r_c , a feature that allows us to compute the probability for the emission of these scalar fields by the black hole, i.e. the so-called greybody factors, by using the asymptotic, free-wave solutions in these two regimes.

The case of a scalar field that is restricted to live on the brane must be studied separately. Such a field propagates strictly in a 4-dimensional gravitational background, that is the projection of the line-element (3) on the brane and follows by fixing the values of the extra angular coordinates, $\theta_i = \pi/2$, for $i = 2, \dots, n+1$. Then, we obtain

$$ds_4^2 = -h(r) dt^2 + \frac{dr^2}{h(r)} + r^2 (d\theta^2 + \sin^2 \theta d\varphi^2), \quad (13)$$

where the metric function $h(r)$ is still given by Eq. (4). A brane scalar field that is coupled to gravity either minimally or non-minimally will now be described by the action functional

$$S_4 = \frac{1}{2} \int d^4x \sqrt{-g} \left[(1 - \xi \Phi^2) R_4 - \partial_\mu \Phi \partial^\mu \Phi \right]. \quad (14)$$

In the above expression, $g_{\mu\nu}$ is the projected metric tensor on the brane defined in Eq. (13), and R_4 the corresponding brane curvature found to be

$$R_4 = \frac{24\kappa_D^2\Lambda}{(n+2)(n+3)} + \frac{n(n-1)\mu}{r^{n+3}}. \quad (15)$$

The brane scalar curvature also carries a dependence on the spacetime parameters but its expression is distinctly different from the bulk one (8).

The variation of S_4 with respect to the brane scalar field Φ now leads to the equation of motion

$$\frac{1}{\sqrt{-g}} \partial_\mu (\sqrt{-g} g^{\mu\nu} \partial_\nu \Phi) = \xi R_4 \Phi. \quad (16)$$

We will assume again a factorized ansatz for the field, namely

$$\Phi(t, r, \theta, \varphi) = e^{-i\omega t} R(r) Y(\theta, \varphi), \quad (17)$$

where $Y(\theta, \varphi)$ are now the usual scalar spherical harmonics. Using the above factorization and the eigenvalue equation of $Y(\theta, \varphi)$, we obtain the following decoupled radial equation for the function $R(r)$ [39]

$$\frac{1}{r^2} \frac{d}{dr} \left(h r^2 \frac{dR}{dr} \right) + \left[\frac{\omega^2}{h} - \frac{l(l+1)}{r^2} - \xi R_4 \right] R = 0. \quad (18)$$

By turning the above equation into a Schrödinger-like form, the brane effective potential is found to be

$$V_{\text{eff}}^{\text{brane}} = h(r) \left\{ \frac{l(l+1)}{r^2} + \frac{4\kappa_D^2\Lambda(6\xi-1)}{(n+2)(n+3)} + \frac{\mu}{r^{n+3}} [(n+1) + \xi n(n-1)] \right\}. \quad (19)$$

The above expression shows a similar behaviour, in terms of the spacetime and scalar field properties, as in the case of the bulk potential but of different magnitude at times. It vanishes again at the two horizons, r_h and r_c , due to the vanishing of the metric function $h(r)$; this will allow us again to study the emission of brane scalar fields by the black-hole background (13). Note that the mass parameter μ can be eliminated from both our bulk and brane analysis by using the black-hole horizon equation $h(r_h) = 0$; then, we obtain

$$\mu = r_h^{n+1} \left(1 - \frac{2\kappa_D^2\Lambda r_h^2}{(n+2)(n+3)} \right). \quad (20)$$

If we then fix the value of the black-hole horizon, i.e. at $r_h = 1$, we may investigate the emission problem of bulk and brane scalar fields in terms of the number of extra dimensions n , cosmological constant Λ , angular-momentum number l and coupling constant ξ of the scalar field.

3 Greybody Factors

In this section, we will determine the greybody factors, i.e. the probability that scalar particles produced near the black-hole horizon will overcome the effective potential barrier and propagate away from the black hole. The analysis must be performed separately

for brane and bulk scalar fields since, as we saw, they ‘see’ a different gravitational background and obey different equations of motion. We will start from the study of scalar fields on the brane since it is this channel of radiation that may be observed, given that the potential observers are also restricted to live on the brane. Subsequently, we will turn to the bulk and perform a similar analysis for higher-dimensional scalar fields.

3.1 Transmission of Scalar Particles on the Brane

The transmission probability for scalar particles propagating in the projected-on-the-brane black-hole background (13) may be found in terms of the radial function $R(r)$. To this end, we need to solve the radial scalar equation (18). Unfortunately, this equation cannot be solved analytically over the whole radial regime even in the absence of the non-minimal coupling parameter ξ or the cosmological constant Λ .

In a previous work of ours [39], Eq. (18) was solved analytically by using an approximate method based on the smooth matching of the asymptotic solutions found by solving the radial equation close to the black-hole and cosmological horizons. Our analysis was a comprehensive one, being valid for all partial modes, labeled by the angular-momentum number l , and taking into account the effect of Λ at both asymptotic regimes. We will now briefly present the main results of our analytic approach as these will be used either as boundary conditions or as checking points for our exact numerical analysis.

The radial equation (18) was first solved in the radial regime close to the black-hole horizon. By using the coordinate transformation

$$r \rightarrow f(r) = \frac{h(r)}{1 - \tilde{\Lambda}r^2}, \quad (21)$$

where $\tilde{\Lambda} \equiv 2\kappa_D^2\Lambda/(n+2)(n+3)$, the aforementioned equation takes the form of a hypergeometric differential equation. Applying the boundary condition that only incoming modes are allowed in the region just outside the black-hole horizon, we obtain the general solution

$$R_{BH}(f) = A_1 f^{\alpha_1} (1 - f)^{\beta_1} F(a_1, b_1, c_1; f), \quad (22)$$

where A_1 is an arbitrary integration constant, while the hypergeometric indices (a_1, b_1, c_1) and the power coefficient β_1 are defined in terms of both particle and spacetime parameters – for more information on this, the interested reader may consult our previous work [39]. Here, we give only the expression of the remaining power coefficient, namely

$$\alpha_1 = -\frac{i\omega r_h}{A_h}, \quad (23)$$

as this will be of use shortly. In the above, $A(r) = (n+1) - (n+3)\tilde{\Lambda}r^2$ and $A_h = A(r = r_h)$.

Near the cosmological horizon, that for a small cosmological constant is located far away from the black-hole horizon, we used instead the simplified metric function $h(r) \simeq 1 - \tilde{\Lambda}r^2$ as the new radial variable. Then, the radial equation (18) in the area

close to $r = r_c$ took again the form of a hypergeometric differential equation with solution

$$R_C(h) = B_1 h^{\alpha_2} (1-h)^{\beta_2} X(a_2, b_2, c_2; h) + B_2 h^{-\alpha_2} (1-h)^{\beta_2} X(a_2 - c_2 + 1, b_2 - c_2 + 1, 2 - c_2; h), \quad (24)$$

where $B_{1,2}$ are also arbitrary constants, and the hypergeometric indices and power coefficients are given again in terms of the parameters of the model.

The matching of the two asymptotic solutions (22) and (24) at an intermediate radial regime ensures the existence of a complete solution in the area between the two horizons. As shown in [39], a smooth matching takes place under the assumption that both the cosmological constant and the non-minimal coupling constant remain small. The amplitudes of the incoming and outgoing wave at the cosmological horizon define the greybody factor for the brane scalar fields; these are found to be given by the integration constants B_1 and B_2 , respectively, and thus the greybody factor, or transmission probability, may be written as

$$|A|^2 = 1 - \left| \frac{B_2}{B_1} \right|^2. \quad (25)$$

The ratio B_2/B_1 follows from the matching of the two asymptotic solutions and is expressed as an analytical, but complicated, expression of all the aforementioned indices, coefficients and parameters of the model [39]. For the case of minimal coupling ($\xi = 0$), and for the lower partial mode ($l = 0$), we have confirmed that, in the limit $\omega \rightarrow 0$, the greybody factor takes the simple form

$$|A^2| = \frac{4r_h^2 r_c^2}{(r_c^2 + r_h^2)^2} + \mathcal{O}(\omega), \quad (26)$$

in terms of the black-hole and cosmological horizons, and in agreement with the results produced in [35, 36, 38]. If we assume instead that $\xi \neq 0$, then the low-energy limit of the greybody factors for all partial modes is of order $\mathcal{O}(\omega r_h)^2$ [39, 38] and therefore vanishes for $\omega \rightarrow 0$. We may thus conclude that the non-vanishing, geometric limit of $|A^2|$ in the low-energy regime is a characteristic of only free, massless scalar particles in a Schwarzschild-de-Sitter spacetime, both four- and higher-dimensional; as soon as we turn on the non-minimal coupling, this feature disappears due to the additional interaction with gravity or, equivalently, due to the existence of an effective mass-term for the scalar field as follows from Eq. (16).

The approximate method described above allowed us to find an expression for the greybody factor fully and explicitly determined by the parameters of system. It also proved to be very satisfying and trustworthy: not only did it reproduce the correct low-energy geometric limit but produced, for most choices of parameters, smooth curves over the entire energy regime, in contrast with other analytic results that usually break down already from the intermediate energy regime. That was due to the fact that we avoided making any unnecessary simplifications or approximations regarding the parameters - not even the energy of the emitted particles - or the mathematical expressions involved. Our only assumptions were the smallness of the cosmological constant Λ and the coupling constant ξ . However, as is usual the case when using this approximate matching

technique, deviations from the exact behaviour are indeed expected to appear when we move beyond the low-energy regime. As a result, in order to be able to compute the complete energy emission spectra for arbitrary choices of our parameters, we should use an exact numerical technique for the integration of Eq. (18) and the derivation of the greybody factor.

We should first determine the boundary conditions for our numerical analysis. Near the black-hole horizon, where $r \rightarrow r_h$ and $f \rightarrow 0$, the corresponding solution (22), takes the form

$$R_{BH} \simeq A_1 f^{\alpha_1} = A_1 e^{-i(\omega r_h/A_h) \ln f}. \quad (27)$$

The above describes indeed an ingoing wave at the black-hole horizon, and, given that the arbitrary constant A_1 carries no physical significance, we may normalize it to unity by setting

$$R_{BH}(r_h) = 1. \quad (28)$$

For the first derivative, we obtain

$$\left. \frac{dR_{BH}}{dr} \right|_{r_h} = A_1 f^{-i(\omega r_h/A_h) \ln f} \left(-\frac{i\omega r_h}{A_h} \right) \frac{A(r)(1-f)}{h(r)r} \Big|_{r=r_h} \simeq -\frac{i\omega}{h(r)}, \quad (29)$$

where, as before, $A(r) = (n+1) - (n+3)\tilde{\Lambda}r^2$ and where we have used Eq. (28) after we performed the derivative.

Although in our analytic approach, the simplified variable $h(r) \simeq 1 - \tilde{\Lambda}r^2$ was used in the regime close to the cosmological horizon, in our numerical analysis, we will keep the f -coordinate (21) as this takes into account the full effect of the black-hole mass and the cosmological constant. Then, following a similar analysis to the one close to the black-hole horizon, the asymptotic solution as $r \rightarrow r_c$ and $f \rightarrow 0$ is written as

$$R_C \simeq B_1 f^{\alpha_2} + B_2 f^{-\alpha_2} = B_1 e^{-i(\omega r_c/A_c) \ln f} + B_2 e^{i(\omega r_c/A_c) \ln f}, \quad (30)$$

where now $\alpha_2 = -i\omega r_c/A_c$. Since f decreases as the cosmological horizon is approached and $A_c < 0$ (as we will see in Section 4), the term proportional to B_1 describes again the ingoing wave and the term proportional to B_2 the outgoing wave. Therefore, the greybody factor is given again by the expression (25).

Our numerical integration starts from the black-hole horizon, i.e. from $r = r_h + \epsilon$, where ϵ is a small positive number in the range $10^{-6} - 10^{-4}$, using the boundary conditions (28)-(29). Note that both the value of ϵ and the integration step are appropriately chosen so that the numerical results are stable. Our numerical integration proceeds towards the cosmological horizon; there, the values of the multiplying coefficients B_1 and B_2 are extracted by using the relations

$$B_1 = \frac{1}{2} e^{i(\omega r_c/A_c) \ln f} \left[R_C(r) + \frac{iA_c h r}{\omega r_c A(r)(1-f)} \frac{dR_C}{dr} \right], \quad (31)$$

$$B_2 = \frac{1}{2} e^{-i(\omega r_c/A_c) \ln f} \left[R_C(r) - \frac{iA_c h r}{\omega r_c A(r)(1-f)} \frac{dR_C}{dr} \right]. \quad (32)$$

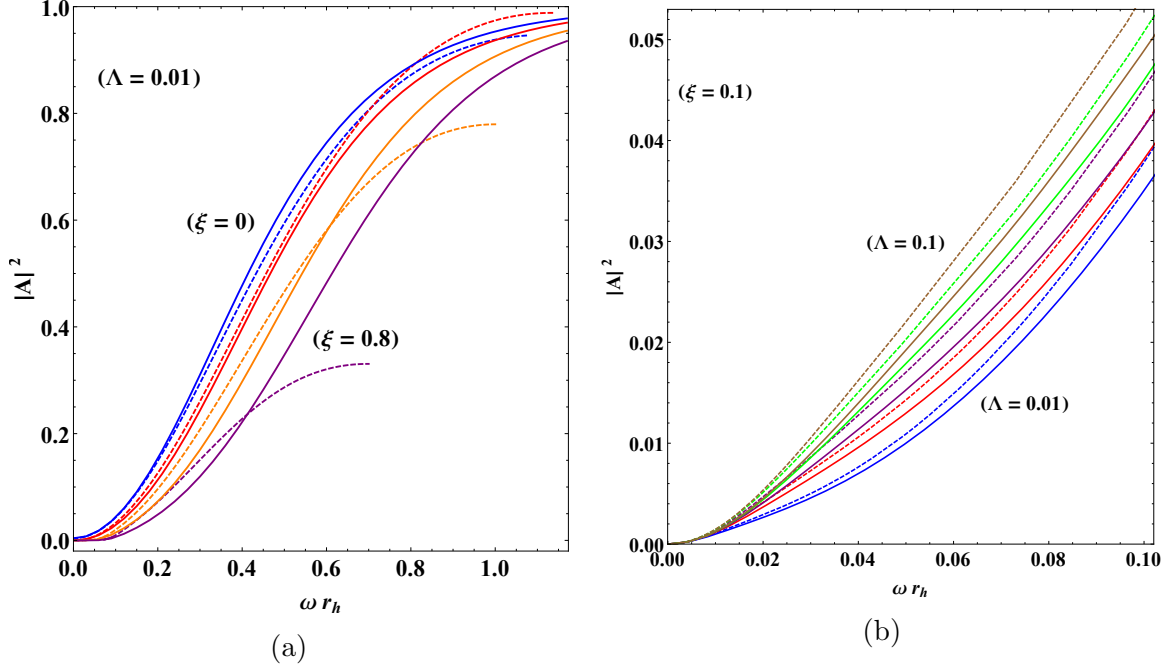


Figure 1: (colour online). Greybody factors for brane scalar fields. Analytical (dashed curves) and numerical results (solid curves) for $l = 0, n = 2$ with (a) $\Lambda = 0.01$ (in units of r_h^{-2}) for variable (top to bottom) $\xi = 0, 0.2, 0.5, 0.8$ and (b) $\xi = 0.1$ for variable (bottom to top) $\Lambda = 0.01, 0.03, 0.05, 0.08, 0.1$.

Having developed our numerical integration technique, we now have the opportunity to check the accuracy of the analytic expressions for the greybody factors derived in our previous work [39]. To this end, in Fig. 1(a,b) we plot the numerical (solid curves) and analytic results (dashed curves) for the greybody factors for brane scalar fields for variable coupling constant ξ and cosmological constant Λ , respectively. As expected, the two sets of results are in excellent agreement in the low-energy regime while for larger values of ωr_h the analytic results deviate from the exact, numerical ones. The deviation depends strongly on the values of ξ and Λ : when both parameters are kept small, the deviation is limited and remains so throughout the energy regime; however, as any of these two parameters increases, the deviation becomes significant and the range of agreement becomes gradually smaller. The latter was anticipated by the fact that our analytic approach was valid only for small values of the parameters ξ and Λ .

We may now use our numerical technique to derive the exact form of the greybody factor for brane scalar fields, that will be valid over the entire energy regime and for arbitrary values of the particle and spacetime parameters. Having the exact greybody factors at our disposal is also a prerequisite for determining the power spectra for the emission of brane scalar fields by a higher-dimensional Schwarzschild-de-Sitter black hole, a task that we undertake in the following section.

In Fig. 2(a), we plot the behavior of the greybody factor under the variation of the angular momentum number l of the field. Clearly, it is the lowest partial mode ($l = 0$) that has the most enhanced greybody factor while higher-field modes have

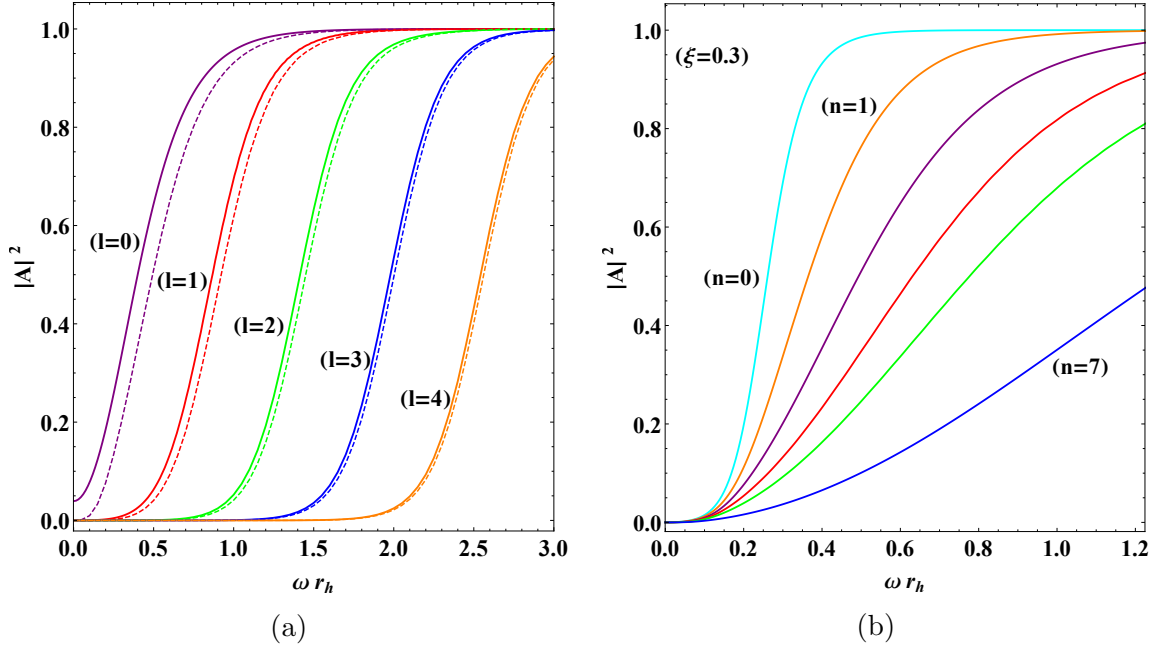


Figure 2: (color online). Greybody factors for brane scalar fields for $\Lambda = 0.1$ and (a) $n = 2$ for variable $l = 0, 1, 2, 3, 4$ and $\xi = 0$ (solid curves) or $\xi = 0.3$ (dashed curves); (b) $l = 0, \xi = 0.3$ for variable (top to bottom) $n = 0, 1, 2, 3, 4, 7$.

their greybody factors suppressed as l increases. This behavior is expected since the background's spherical symmetry favors the emission of modes with the same type of symmetry. The plot depicts also the dependence of the greybody factor for minimal and non-minimal coupling: in the case of the $l = 0$ mode, the non-vanishing asymptotic low-energy limit (26) is recovered for $\xi = 0$, while for non-vanishing ξ , this asymptotic value vanishes. In all cases, the effect of the coupling constant is to suppress the greybody factor throughout the energy regime. This effect is more prominent for the lower partial modes and is almost entirely eliminated for $l \geq 4$. The above behaviour is in excellent agreement with the analytic one found in [39] for small values of l and in the low-energy regime; however, as either parameter increases the analytic results suffer from the appearance of poles that occasionally lead to the abrupt termination of the greybody factor curve. The exact numerical analysis overcomes this obstacle and provides us with complete, smooth curves.

In Fig. 2(b), we depict the dependence of the greybody factor on the number of extra spacelike dimensions n . In various previous works, it has been noted that n causes a suppression of the greybody factor for brane scalar fields over the entire energy regime, and we recover the same behaviour here. Comparison of the exact numerical results with the analytic ones of [39] reveal again a very good agreement at the low-energy regime. As either the energy parameter or the number of dimensions increases, the range of agreement decreases, and the analytic curves, due again to the existence of poles, tend to lie “lower” than the exact numerical ones, a behaviour that is found to be common in all subsequent plots.

We now turn to the dependence of the greybody factor on the two important pa-

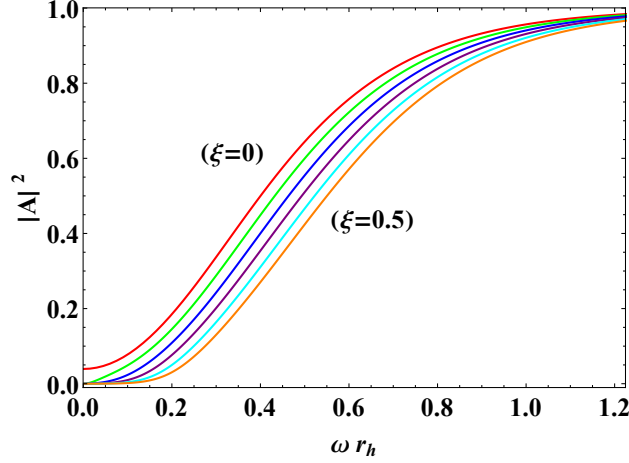


Figure 3: (color online). Greybody factors for brane scalar fields for $l = 0$, $n = 2$, $\Lambda = 0.1$ and variable (top to bottom) $\xi = 0, 0.1, 0.2, 0.3, 0.4, 0.5$.

rameters of our model, the non-minimal coupling constant of the scalar field and the cosmological constant of spacetime. In Fig. 3, we plot the dependence of the greybody factor on ξ for the dominant mode ($l = 0$) and for fixed cosmological constant ($\Lambda = 0.1$) and number of extra dimensions ($n = 2$). From the equation of motion (16) of the brane scalar field, we may interpret the coupling term of the scalar field to the curvature scalar R_4 as an effective mass term for Φ – this has been noted before in [38, 39]. As a result, the increase in the value of ξ corresponds to an increased effective mass, and thus to a suppressed transmission probability for the particle, as found before in [45, 46, 47, 48]. This is in perfect agreement with the behaviour depicted in Fig. 3, where the greybody factor gets suppressed the higher the value of ξ becomes. Once again, for the minimal coupling case of $\xi = 0$, the non-vanishing low-energy asymptotic limit (26) is recovered as expected.

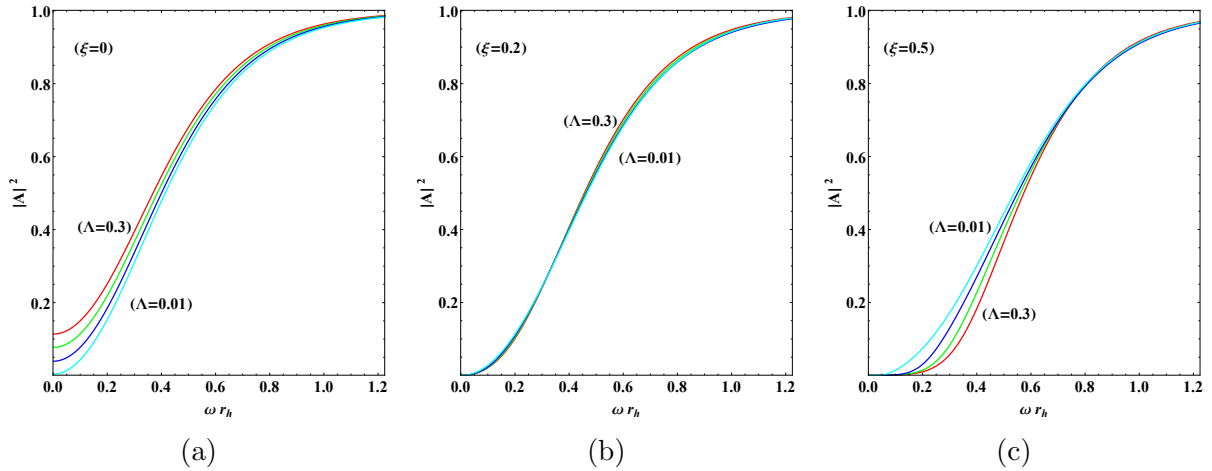


Figure 4: (colour online). Greybody factors for brane scalar fields for $l = 0$, $n = 2$ and $\Lambda = 0.01, 0.1, 0.2, 0.3$ and (a) for $\xi = 0$, (b) $\xi = 0.2$ and (c) $\xi = 0.5$.

The effect of the cosmological constant on the greybody factor, as was discussed in [39], depends on the value of the coupling constant ξ . In Fig. 4, we plot $|A|^2$ for four different values of Λ and three different values of ξ . For the minimal-coupling case, depicted in Fig. 4(a), larger values of the cosmological constant enhance the greybody factor throughout the energy regime. For the intermediate value $\xi = 0.2$ [see Fig. 4(b)], the greybody factors exhibit a slight interchange of behaviour at the intermediate-energy regime but an extremely soft dependence on Λ altogether. As the coupling constant ξ increases further, we see from Fig. 4(b) that the role of Λ is now reversed, and larger values of the cosmological constant lead to a suppression in the greybody factor especially in the low-energy regime. As noted in [39], this subtle behaviour is due to the two different contributions of Λ : for small values of ξ , the suppression due to the mass term (that is proportional also to Λ) is small and the cosmological constant, as part of the metric function, subsidizes the transmission probability of the brane scalar field through the potential barrier (19) [35]; for intermediate values of ξ , the two contributions almost cancel each other, while for large values of ξ , the effective mass increases substantially leading to the suppression of $|A|^2$ in terms of Λ .

3.2 Transmission of Scalar Particles in the Bulk

Scalar particles that propagate in the higher-dimensional gravitational background (3) obey the equation of motion (9). The greybody factor may be determined in this case by solving the radial equation (11). This equation was also solved analytically in [39] by following a similar approximate method. In fact, the asymptotic solutions near the black-hole and cosmological horizons take the exact same forms as (22) and (24), respectively, differing only in the definition of the hypergeometric indices and in the power coefficients [39] – in fact the power coefficient α_1 adopts exactly the same functional form (23) as in the brane emission.

Apart from the above modifications, the procedure that was followed was the same as for propagation on the brane. The matching of the two asymptotic solutions led again to an analytic expression for the ratio B_2/B_1 and, through Eq. (25), for the greybody factor for bulk scalar fields. This expression was shown again to correctly reproduce, for the minimal-coupling case, the non-vanishing, geometric, low-energy limit for $|A|^2$ for the mode $l = 0$ found in [35] and now given by

$$|A^2| = \frac{4(r_h r_c)^{(n+2)}}{(r_c^{n+2} + r_h^{n+2})^2} + \mathcal{O}(\omega). \quad (33)$$

Comparing the above expression with the one on the brane (26), we observe that the presence of the number of extra dimensions n in the exponents of r_h and r_c causes the magnitude of the low-energy asymptotic value in the bulk to be significantly smaller compared to the one on the brane. For $\xi \neq 0$, the greybody factors for all modes of the bulk scalar field reduce again to zero [39].

Once again, the smooth matching of the asymptotic solutions was achieved under the assumptions of small cosmological constant and small coupling constant. As a result, we turn again to the numerical integration of the radial equation (11) in order to produce

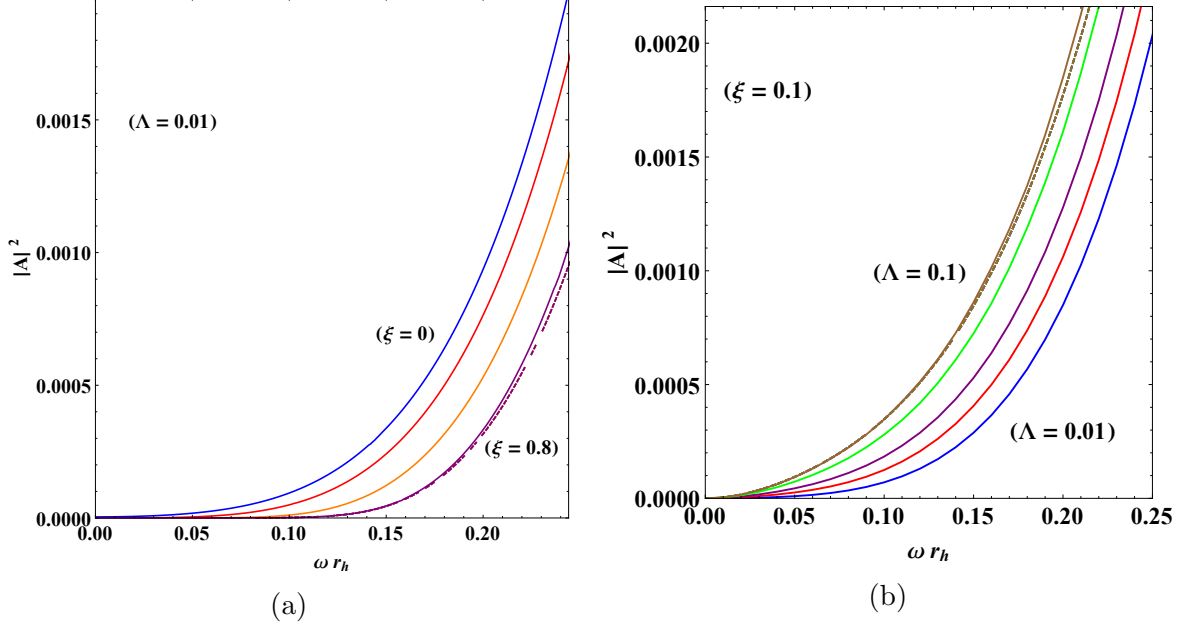


Figure 5: (colour online). Greybody factors for bulk scalar fields. Analytical (dashed curves) and numerical (solid curves) results for $l = 0, n = 2$ and: (a) for $\Lambda = 0.01$ and variable $\xi = 0, 0.2, 0.5, 0.8$; (b) for $\xi = 0.1$ and variable $\Lambda = 0.01, 0.03, 0.05, 0.08, 0.1$.

exact, complete results for the greybody factor. Given that the asymptotic solutions near the black-hole and cosmological horizons are the same for brane and bulk propagation, the same holds true for their expanded forms (27) and (30) and the boundary conditions for the numerical integration (28)-(29). Once again, the integration starts from the proximity of the black-hole horizon and proceeds to the cosmological horizon where the amplitudes of the incoming and outgoing modes are isolated and determined through Eqs. (31)-(32). The exact value of the greybody factor, for arbitrary values of the particle and spacetime parameters, is then found via Eq. (25).

For completeness, the comparison of analytical and numerical results for $|A|^2$ for scalar fields in the bulk is presented in Figs. 5(a,b) in terms of the coupling constant ξ and cosmological constant Λ , respectively. An excellent agreement is observed between the exact (dashed) and the analytical (solid) results for the greybody factors that persists beyond the low-energy regime. As the values of either ξ or Λ become larger, deviations appear, as expected, and the validity regime of the analytic results becomes smaller.

Turning now to the complete, exact results, in Fig. 6(a) we depict the dependence of the greybody factor for scalar fields in the bulk in terms of the angular momentum number l , for $n = 2$ and $\Lambda = 0.1$ (in units again of r_h^{-2}). The suppression of $|A|^2$ as the partial mode number increases is observed for both cases of minimal (solid curves) and non-minimal (dashed curves) coupling; however, the difference is less noticeable than the one observed in the case of brane propagation, even for small values of l . Our exact numerical analysis has led to the complete greybody curves in contrast to our previous analytic study where these curves were restricted to the very low-energy regime due to the existence of poles. Because of the smallness of the asymptotic geometric value of

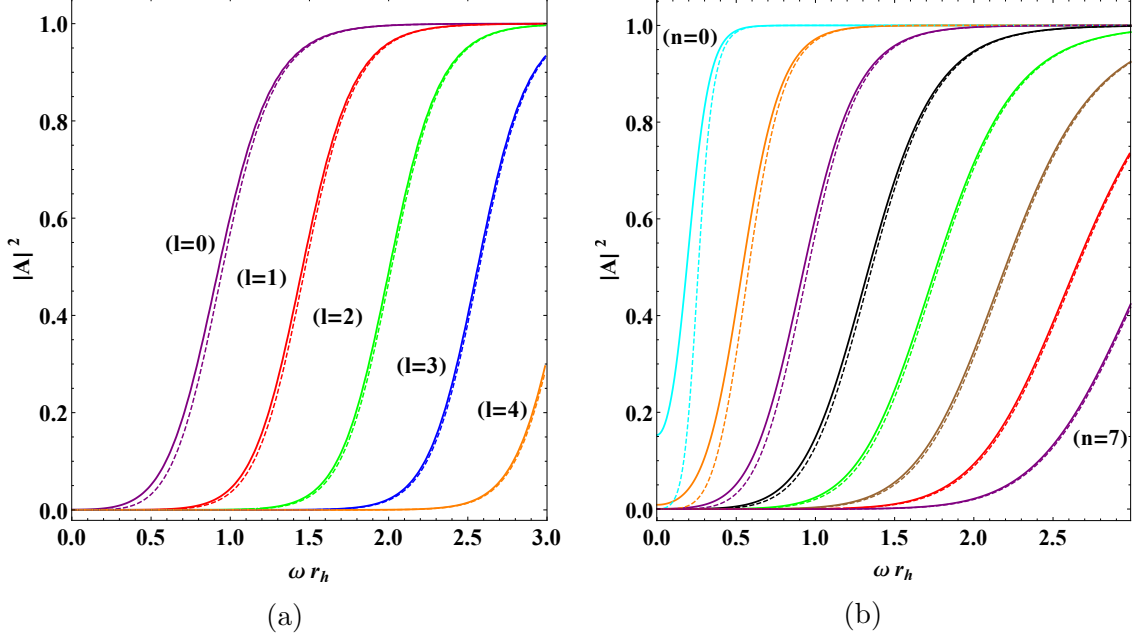


Figure 6: (color online). Greybody factors for bulk scalar fields for $\Lambda = 0.1$, $\xi = 0$ (solid curves) or $\xi = 0.3$ (dashed curves) and: (a) $n = 2$ and variable $l = 0, 1, 2, 3, 4$; (b) $l = 0$ and variable $n = 0, 1, 2, 3, 4, 5, 6, 7$.

$|A|^2$ for the lowest mode $l = 0$ in the limit $\omega \rightarrow 0$ for the case $n = 2$, the difference between the minimal and non-minimal coupling cases can not be discerned in Fig. 6(a) – a zoom-in plot of the low-energy regime would be necessary to achieve this.

This difference is however visible in Fig. 6(b), where we show the dependence of the greybody factor on n for the dominant mode with $l = 0$: for the two lowest values, $n = 0$ and $n = 1$, the difference in the low-energy asymptotic values of $|A|^2$, as we turn on or off the coupling constant ξ , may be clearly seen. In general, the greybody factor is universally suppressed, as the number of extra spacelike dimensions increases, and the scalar particle is less likely to overcome the potential barrier. Note that our exact numerical analysis has provided us with results for all values of n , in contrast to our analytic approach where results for only even values of n were derived due to the existence again of poles.

In Fig. 7, the dependence of the greybody factor on the coupling constant ξ is depicted for the dominant mode ($l = 0$). We observe that, in the bulk, in contrast to the brane emission, for the same choice of parameters, the effect of the variation in ξ is milder – this is justified by the fact that the dependence of the bulk potential barrier on ξ is also very mild as was shown in [39]. Still, as the coupling constant increases, the greybody factor gets suppressed; this behavior can be once again interpreted as the result of the increased effective mass of the field generated through its coupling to the Ricci scalar.

The effect of the cosmological constant on the greybody factor for bulk scalar fields is shown in Fig. 8: the minimal coupling case is given in Fig. 8(a) while a non-vanishing value of the field coupling ($\xi = 0.5$) is employed in Fig. 8(b). The dual role of the cosmological constant – contributing simultaneously to the lowering of the potential

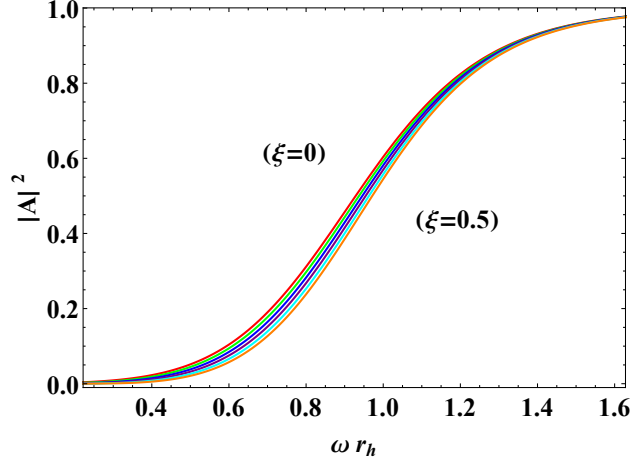


Figure 7: (color online). Greybody factors for bulk scalar fields for $n = 2, \Lambda = 0.1, l = 0$ and variable $\xi = 0, 0.1, 0.2, 0.3, 0.4, 0.5$.

barrier and to the effective field mass – is again clear. Although the dependence of $|A|^2$ on Λ is in general soft, for vanishing or small values of the coupling constant ξ , the greybody factor is enhanced with the cosmological constant; for larger values of ξ though, the situation is reversed, mainly in the low and intermediate-energy regime, where an increase in Λ suppresses the greybody factor. It is worth noting that a very good agreement is found between the numerical results presented here and the analytical ones derived in [39] regarding the role of the cosmological constant.

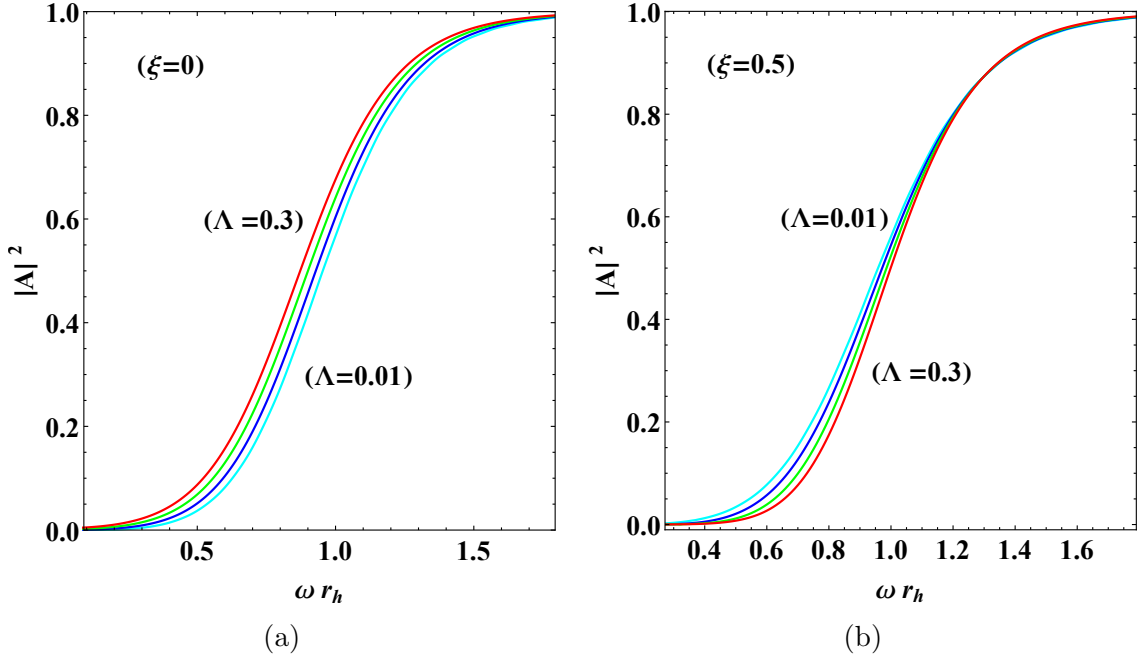


Figure 8: (colour online). Greybody factors for bulk scalar fields for $l = 0, n = 2$ and $\Lambda = 0.01, 0.1, 0.2, 0.3$ and (a) for $\xi = 0$ and (b) $\xi = 0.5$.

Finally, let us finish this section by making the following observations: by mere comparison of Figs. 2(a,b) and 6(a,b) depicting the dependence of the greybody factors for brane and bulk scalar fields, respectively, on l and n – a comparison made easy by our selecting on purpose the same sets of parameters – one may see that the suppression of $|A|^2$ with both l and n is much more important for bulk rather than for brane propagation. This effect is a well-known one leading to the dominance of the brane over the bulk channel when one studies the emission of scalar fields by a higher-dimensional Schwarzschild black hole [5, 6]. However, in the present analysis we have two more parameters, the coupling constant of the scalar field and the cosmological constant of the spacetime background. Regarding the former, we may again observe, from Figs. 3 and 7, that the suppression it causes to the value of the greybody factor is more prominent for brane scalars than for bulk scalars. Will the effect of the non-minimal coupling constant be able to undermine the dominance of the brane emission channel? And, will the cosmological constant with its subtle effect, despite the soft dependence of the greybody factor on it, be able to affect in any way the bulk-to-brane energy balance? We will return to those questions at the final part of the following section.

4 Energy Emission Rates

We now proceed to the derivation of the differential energy emission rates by a higher-dimensional Schwarzschild-de-Sitter black hole in the form of scalar fields. We will study the emission of scalar Hawking radiation both on the brane and in the bulk and, subsequently, discuss the total emissivity of each channel and their relative ratio in order to investigate whether the additional parameters of the model, the coupling constant and the cosmological constant, may change the energy balance between brane and bulk.

4.1 Power Spectra for Emission on the Brane

We start with the emission of scalar particles on the brane. The differential energy emission rate is given by the expression [6, 24, 35]

$$\frac{d^2 E}{dt d\omega} = \frac{1}{2\pi} \sum_l \frac{N_l |A|^2 \omega}{\exp(\omega/T_{BH}) - 1}, \quad (34)$$

where ω is the energy of the emitted, massless particle, $|A|^2$ the greybody factor, or transmission probability, computed in the previous section, and $N_l = 2l + 1$ the multiplicity of states that, due to the spherical symmetry, have the same angular-momentum number. Also, T_{BH} is the temperature of the black hole determined through the surface gravity as

$$T_{BH} = \frac{k_H}{2\pi} = \frac{1}{4\pi r_h} \left[(n+1) - \frac{2\kappa_D^2 \Lambda r_h^2}{(n+2)} \right], \quad (35)$$

where Eq. (20) has been used to eliminate any dependence on the mass parameter μ . However, here we will follow the Bousso-Hawking definition of the temperature since Eq. (35) is strictly valid only when the spacetime is asymptotically flat [49]. For the

Schwarzschild-de-Sitter spacetime, though, this does not hold; the only point where “asymptotic flatness” may be considered to hold is at the point r_0 located between r_h and r_c where the effects of black-hole attraction and cosmological repulsion cancel out. This point corresponds to an extremum of the metric function $h(r)$ and is found to be

$$r_0 = \left[\frac{(n+1)(n+2)(n+3)\mu}{4k_D^2\Lambda} \right]^{1/(n+3)}. \quad (36)$$

Therefore, the correct definition of the temperature of a Schwarzschild-de-Sitter black hole is the following [35, 49]

$$T_{BH} = \frac{k_H}{2\pi} = \frac{1}{\sqrt{h(r_0)}} \frac{1}{4\pi r_h} \left[(n+1) - \frac{2k_D^2\Lambda r_h^2}{(n+2)} \right]. \quad (37)$$

Note that, as expected, when the cosmological constant tends to zero, the point r_0 moves to infinity: there, the metric function becomes unity, the normalising factor $1/\sqrt{h(r_0)}$ disappears and Eq. (37) gives the well-known expression for the temperature of a higher-dimensional Schwarzschild black hole ¹.

We now have all the tools to compute the energy emission rate on the brane: using Eqs. (34) and (37) and the exact numerical results for the greybody factor derived in Section 3.1, we may investigate the dependence of the spectrum on all the particle and spacetime properties. The contribution to the energy emission rate comes mainly from the dominant modes of the scalar field namely the ones with the lowest values of l . As l increases, the l -th mode contributes less and less to the total spectrum. We took advantage of this fact to terminate the infinite sum in Eq. (34) at a finite number of modes. More precisely, we found that all modes higher than the $l = 7$ mode contribute an amount which is many orders of magnitude lower than the peak of the power curve, and so we may safely ignore them. An indicative example of this behaviour is shown in Fig. 9 for $n = 2$, $\Lambda = 0.1$ and $\xi = 0$: clearly, as l increases, the modes contribute less to the total sum with the $l = 5$ mode being already irrelevant.

The dependence of the energy emission rate for brane scalars on the number of extra spacelike dimensions is depicted in Fig. 10(a). Clearly, the energy emitted by the black hole per unit time and unit frequency on the brane is enhanced with n ; this feature was noted before in [35] where the emission of a Schwarzschild-de-Sitter black hole was also studied as well as in a number of previous works on both spherically and axially symmetric black holes [5]-[16]. Although the greybody factor, as shown in section 3.1, gets suppressed with the number of extra dimensions, the temperature of the black hole (35) gets significantly enhanced leading at the end to the overall enhancement of the power spectra.

On the other hand, as the temperature of the black hole is insensitive to the particle properties, we expect the suppression of the greybody factor with the value of the non-minimal coupling constant to carry on to the energy emission rate. From Fig. 10(b), we

¹The temperature of the universe T_C is also given by an expression similar to Eq. (35) with r_h being replaced by r_c and an overall minus sign introduced to ensure the positivity of T_C . The latter may be alternatively written as $T_C = -A_c/4\pi r_c$, therefore the quantity A_c is negative as used in Section 3.1. Finally, one may easily conclude that $T_{BH} > T_C$, therefore it is only the emission from the black-hole horizon that is relevant here.

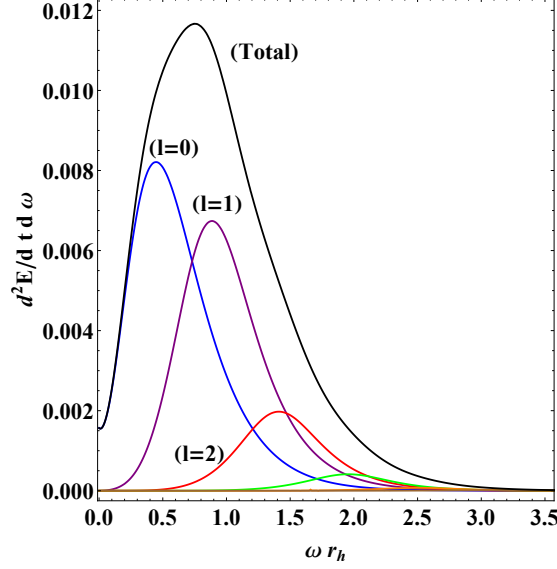


Figure 9: (color online). Energy emission rate curves for brane scalar fields for $n = 2$, $\Lambda = 0.1$, $\xi = 0$ for the first five dominant modes with $l = 0, 1, 2, 3, 4, 5$.

observe that this is indeed the case: as ξ increases, the power spectra are suppressed throughout the energy regime. This picture is also consistent with the interpretation of the non-minimal coupling term of the scalar field to the Ricci curvature as an effective mass term: in [48], the power spectra for massive scalar fields were derived and the similarity between those results and the behaviour depicted in Fig. 10(b) is striking; in both analyses, the emission curves adopt non-zero values at a gradually larger value of

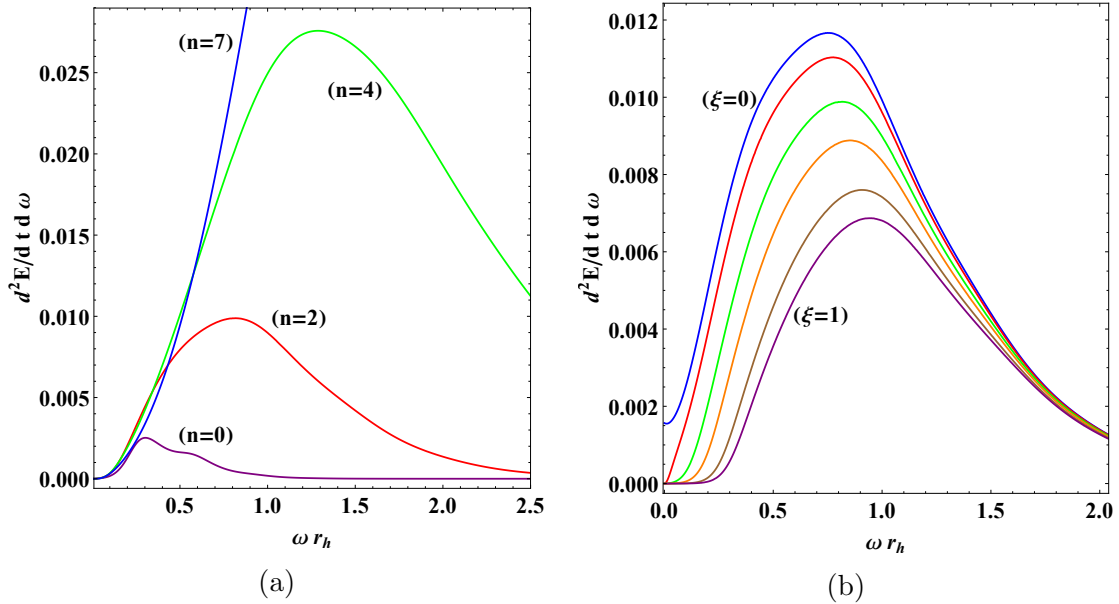


Figure 10: (colour online). Energy emission rates for brane scalar fields, for $\Lambda = 0.1$, and: (a) $\xi = 0.3$ and variable $n = 0, 2, 4, 7$; (b) $n = 2$ and variable $\xi = 0, 0.1, 0.3, 0.5, 0.8, 1$.

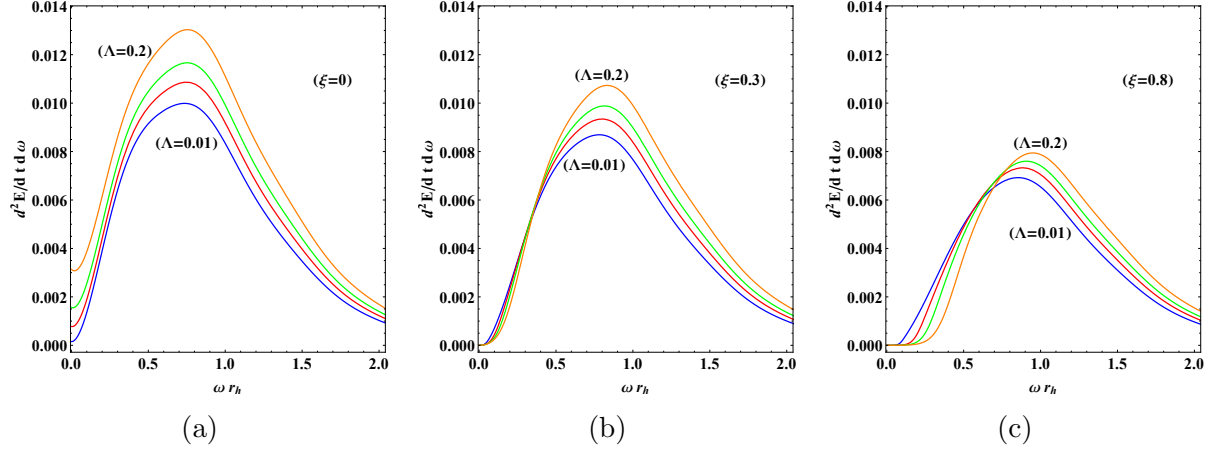


Figure 11: (colour online). Energy emission rates for brane scalar fields for $n = 2$, variable $\Lambda = 0.01, 0.05, 0.1, 0.2$, and for: (a) $\xi = 0$, (b) $\xi = 0.3$, and (c) $\xi = 0.8$.

ωr_h as the mass increases, exhibit a uniform suppression over the whole energy regime and converge to a common “tail” at the high-energy regime.

In Fig. 10(b), we also observe that for the case of minimal coupling, i.e. for $\xi = 0$, the energy emission curve starts from a non-vanishing low-energy value. This feature was first found in [35] and later confirmed in [36, 37, 38]: it is attributed to the non-vanishing, geometric, low-energy value of the greybody factor for scalar fields and leads to a non-zero probability for the emission of scalar particles with extremely low energy on the brane. The same behaviour is depicted in Fig. 11(a), where the emission curves for the minimal coupling case and for various values of the cosmological constant are shown. Again, the results derived previously in the aforementioned works are confirmed: as Λ increases, the energy emission rate is uniformly enhanced and the same holds for its asymptotic value at the very low-energy regime.

However, as soon as the non-minimal coupling constant takes non-vanishing values, the situation changes radically also for the power spectra: the low-energy asymptotic value of the emission rate is now zero and the dependence on the cosmological constant depends both on the value of ξ and the energy regime. For intermediate values of ξ , as displayed in Fig. 11(b), the enhancement in terms of Λ appears only in the intermediate and high-energy regime and is of a smaller magnitude. For larger values of ξ , as in Fig. 11(c), the emission rate is even less enhanced in the aforementioned regimes while at the low-energy regime is actually suppressed in terms of Λ .

4.2 Power Spectra for emission in the bulk

The differential energy emission rate for the Hawking radiation in the form of bulk scalar fields is again given by Eq. (34). Bulk and brane modes “see” the same black-hole temperature (37), however, the multiplicity of states that correspond to the same angular-momentum number is now different: due to the enhanced spherical symmetry of

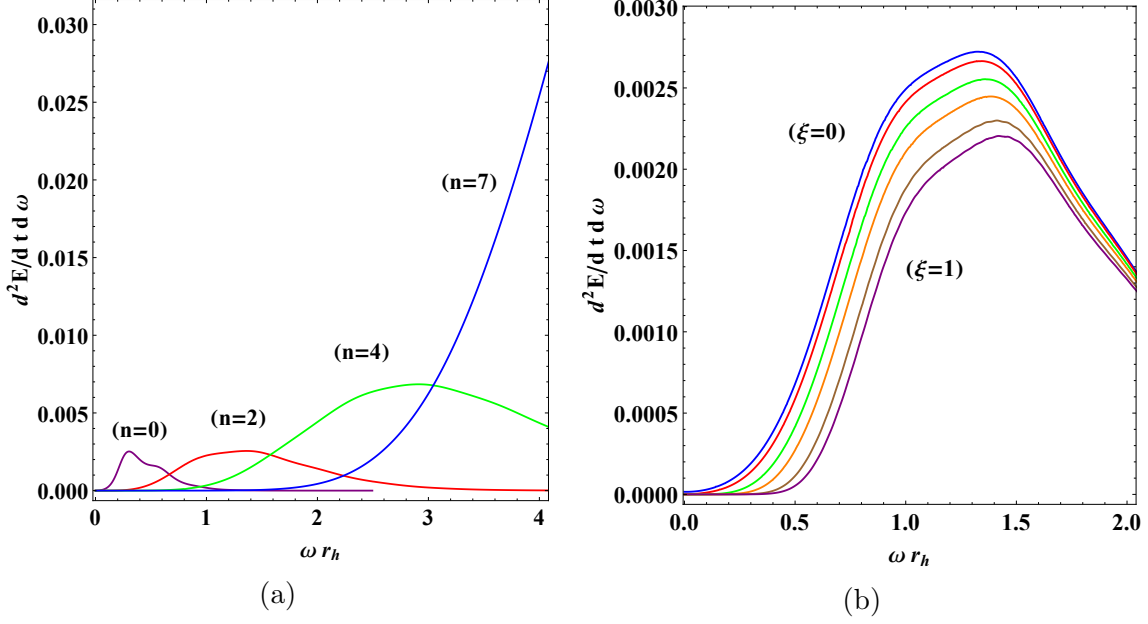


Figure 12: (colour online). Energy emission rates for bulk scalar fields for $\Lambda = 0.1$, and: (a) $\xi = 0.3$ and variable $n = 0, 2, 4, 7$; and (b) $n = 2$ and variable $\xi = 0, 0.1, 0.3, 0.5, 0.8, 1$.

the $(4 + n)$ -dimensional spacetime, N_l is now given by [50, 35]

$$N_l = \frac{(2l + n + 1)(l + n)!}{l!(n + 1)!}. \quad (38)$$

Another important difference is, of course, the expression for the greybody factor $|A|^2$ that now describes the transmission of scalar fields through the bulk potential barrier. In order to derive the complete, exact power spectra for emission of bulk scalar fields, the numerical results for the corresponding greybody factor found in Section 3.2 will be used.

In Fig. 12(a), we depict the dependence of the energy emission rate for scalar fields in the bulk in terms of the number of extra dimensions. The peaks of the energy emission curves are shifted towards larger frequencies, in a more prominent way compared to the case of brane emission, and their heights increase leading again to a significant enhancement with the number of extra dimensions. A comparison of Figs. 10(a) and 12(a) shows that the bulk emission curves lie lower than the corresponding brane emission curves pointing to the dominance of the brane over the bulk emission channel – however, this holds for the particular sets of parameters chosen while, as we will see in the next subsection, a different set of parameters may reveal an altogether different picture.

The expected suppression of the power spectra in terms of the coupling constant ξ is indeed observed in Fig. 12(b), also for the bulk scalar fields. The general profile of the emission curves, as ξ varies, is again in complete agreement with the behaviour of the energy emission curves for bulk, massive particles [48] as their mass changes. Note, that in the case of minimal coupling, we should also observe a non-vanishing asymptotic emission rate as the energy goes to zero; however, the smallness of the corresponding

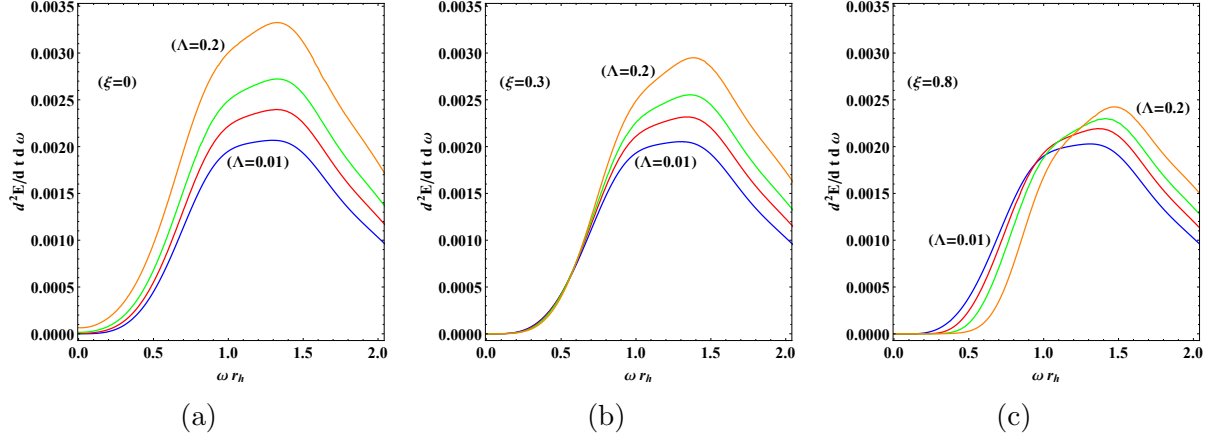


Figure 13: (colour online). Energy emission rates for bulk scalar fields for $n = 2$, variable $\Lambda = 0.01, 0.05, 0.1, 0.2$, and for: (a) $\xi = 0$, (b) $\xi = 0.3$, and (c) $\xi = 0.8$.

asymptotic value of the greybody factor for bulk scalar fields, for the particular value of Λ chosen (i.e. $\Lambda = 0.1$), leads to the small value of the energy emission rate, and a zoom-in plot would be again necessary to observe this.

This feature is more easily seen in Fig. 13(a), depicting the minimal-coupling case with $\xi = 0$, where a larger value has been chosen for the cosmological constant for the upper curve (i.e. $\Lambda = 0.2$). Also, in this case, we may see the enhancement of the power spectra over the whole energy regime as the cosmological constant increases. As the coupling constant takes on non-vanishing values, we observe a similar behaviour to the one for brane emission: for moderate values of ξ , the enhancement is restricted in the intermediate and high-energy regimes, while for larger values of ξ , the high-energy, limited enhancement is accompanied by a low-energy suppression in terms of Λ – see Figs. 13(b,c), respectively.

4.3 Bulk versus Brane: Relative Emission Rates and Total Emissivities

In this final subsection, we compare the relative emission rates of the higher-dimensional Schwarzschild-de-Sitter black hole in the bulk and on the brane. We will demonstrate that the parameters of this model affect significantly the amount of energy emitted on the brane compared to the one in the bulk, and, for certain ranges of parameters, they can even tilt the energy balance in favour of the bulk channel.

The effect of the field coupling ξ on the bulk-to-brane energy emission ratio is given in Fig. 14(a), where we have fixed the number of extra dimensions and value of cosmological constant to $n = 4$ and $\Lambda = 0.1$, respectively. The coupling constant ξ assumes a dual role, depending on which part of the energy spectrum we consider: at the low-energy regime, a large value of the coupling favours the brane emission while beyond the intermediate regime, is the bulk emission that is now enhanced. Indeed, an inspection of Figs. 10 and 12 clearly shows that, for the same choice of parameters, the bulk emission at the

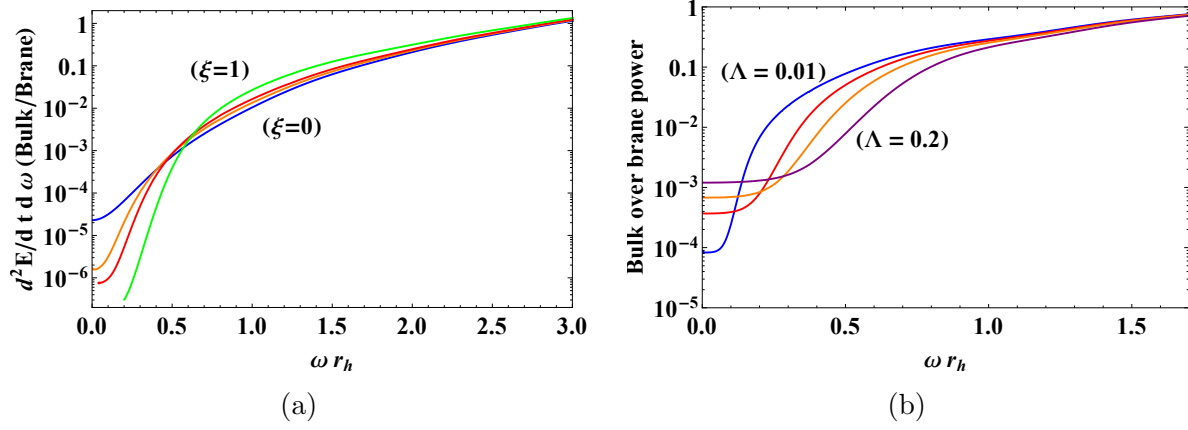


Figure 14: (colour online). Bulk-over-brane relative emission rates for: (a) $n = 4$, $\Lambda = 0.1$ and variable $\xi = 0, 0.3, 0.5, 1$, and (b) $\xi = 0.8$, $n = 2$ and variable $\Lambda = 0.01, 0.05, 0.1, 0.2$.

low-energy regime is very much suppressed compared to the brane one, and this pushes the bulk-to-brane ratio to extremely small values; at the high-energy regime, though, the same plots reveal that the two energy emission rates differ by, at most, an order to magnitude or even less depending on the values of n , Λ and ωr_h . According to Fig. 14(a), the bulk-to-brane ratio remains smaller than unity but it is clearly pushed to values close to, or even above, unity at the high-energy regime. This is again in agreement with the role that the mass of a scalar field plays in the bulk-to-brane ratio: as was shown in [48], the mass of the scalar field gives a significant boost to the bulk channel.

According to the behaviour depicted in Fig. 14(b), the cosmological constant plays a similar dual role: at the very low-energy regime, an increase in its value seems to enhance the bulk channel, at the intermediate regime it is the brane channel that is enhanced instead, while at the high-energy regime the bulk-to-brane ratio becomes almost insensitive to the value of the cosmological constant. This change of role is due to the presence of the coupling constant which here has been given the value $\xi = 0.8$; in the minimal coupling case, studied in [35], the increase in the value of Λ led to the enhancement of the bulk channel throughout the low and intermediate-energy regime. Again, for the range of parameters shown in this plot, the energy ratio seems to approach unity as the energy parameter increases further, and, as a result, highly-energetic particles have equal emission rates on the brane and in the bulk.

Last, but not least, we should address also the effect that the number of extra dimensions has on the value of the bulk-to-brane ratio. In [35], where the minimal coupling case was studied, it was demonstrated that, up to the intermediate energy regime, the bulk-to-brane ratio remained below unity, and it actually decreased as n increased. This is the behaviour we obtain also in Fig. 15, where the coupling constant has now adopted a moderate, non-vanishing value ($\xi = 0.3$). At the low and intermediate-energy regime, there is a clear brane emission domination; however, at larger frequencies the curves for different values of n cross each other revealing an enhancement in the emission of bulk scalars over brane scalars with the number of extra dimensions. Finally, at high energies, the bulk emission is clearly favored over the brane one for all values of n , and the bulk

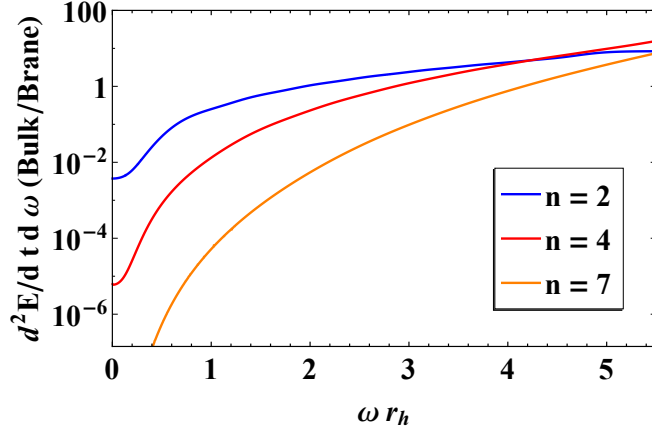


Figure 15: (color online). Bulk-over-brane relative emission rates for $\xi = 0.3$, $\Lambda = 0.2$ and variable $n = 2, 4, 7$.

channel dominates.

As an indicative example of the combined effect that the number of extra dimensions, cosmological constant and non-minimal coupling may have on the emission rates, in Figs. 16(a,b), we depict the bulk and brane emission curves for $n = 7$, $\Lambda = 0.2$ and for two different values of the coupling constant, $\xi = 0.3$ and $\xi = 1$, respectively. For the former value of ξ , Fig. 16(a) justifies several of the features already discussed in Fig. 15: for this

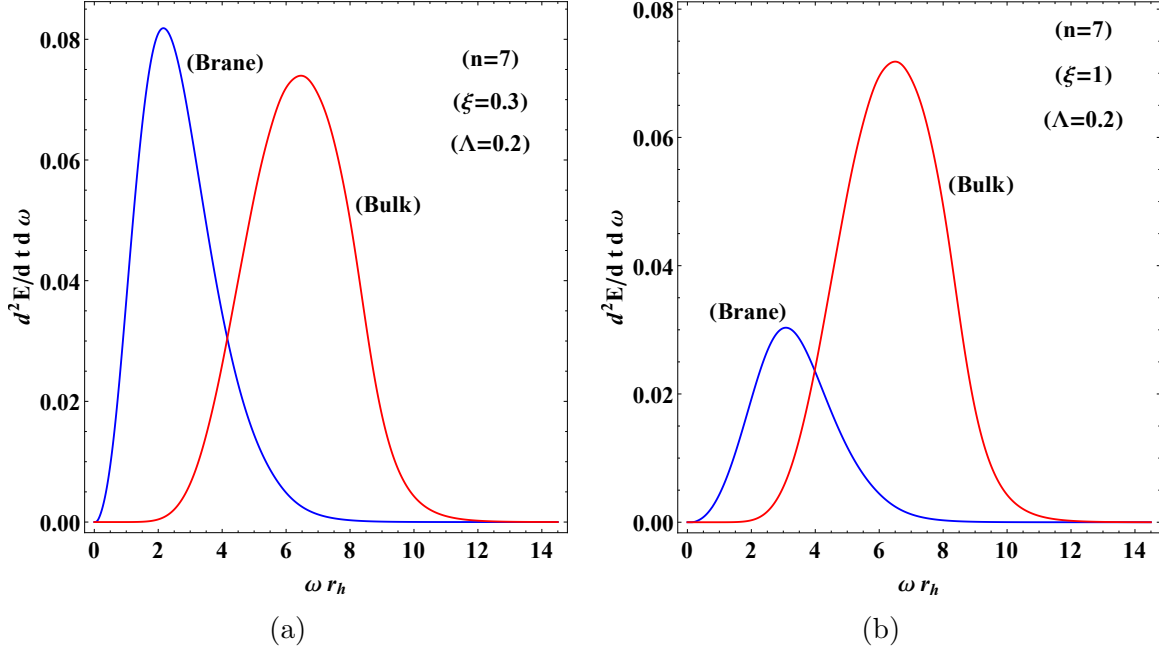


Figure 16: (color online). Power spectra for emission on the brane and in the bulk for $n = 7$, $\Lambda = 0.2$, and: (a) $\xi = 0.3$, and (b) $\xi = 1$.

Table 1: Bulk over brane total emissivity for $n = 2$

$\xi \rightarrow$	0.0	0.1	0.3	0.5	0.8	1.0
$\Lambda = 0.01$	0.257506	0.269481	0.294391	0.320639	0.362918	0.393068
0.05	0.27356	0.285502	0.309271	0.333195	0.369824	0.394932
0.1	0.288635	0.300295	0.322187	0.343	0.373032	0.392523
0.2	0.314566	0.325492	0.343106	0.357599	0.375749	0.38618

Table 2: Bulk over brane total emissivity for $n = 4$

$\xi \rightarrow$	0.0	0.1	0.3	0.5	0.8	1.0
$\Lambda = 0.01$	0.247028	0.275432	0.339321	0.413966	0.549627	0.658426
0.05	0.255885	0.284767	0.349056	0.423319	0.556669	0.662449
0.1	0.264557	0.293826	0.358134	0.43146	0.561241	0.662884
0.2	0.279594	0.30942	0.373259	0.444156	0.566328	0.659702

Table 3: Bulk over brane total emissivity for $n = 7$

$\xi \rightarrow$	0.0	0.1	0.3	0.5	0.8	1.0
$\Lambda = 0.01$	0.779006	0.906992	1.21479	1.60427	2.38062	3.05751
0.05	0.790883	0.92003	1.22955	1.61993	2.39509	3.0686
0.1	0.803103	0.933293	1.24413	1.63466	2.40657	3.07444
0.2	0.824629	0.956511	1.26906	1.65866	2.42208	3.07722

set of parameters, the brane emission is indeed dominant at the low-energy regime but the bulk dominates in the emission of high-energy modes. As ξ adopts the latter value, Fig. 16(b) reveals a picture with the same qualitative profile but with a fundamental difference from the quantitative point of view: the dominance of the bulk emission is now so strong that the emission on the brane seems to comprise only a small part of the total black-hole emission.

The aforementioned behaviour makes imperative the calculation and comparison of the brane and bulk total emissivities, i.e. the amount of energy emitted by the black hole on the brane and in the bulk in the unit of time over the whole frequency range. To this end, we integrate the differential energy emission rate (34) over the frequency ω ; this is equivalent to computing the area under the energy emission curves. We perform this for a range of values of our parameters, and at the end we compute the bulk-to-brane ratio of emissivities; this ratio will be a good index of how the energy balance between brane and bulk changes in terms of the parameters. The obtained values are displayed in Tables 1 through 3.

Starting from the minimal-coupling case with $\xi = 0$, we observe that, independently of the value of Λ , the bulk-to-brane emissivity ratio takes a dip for intermediate values of n , and then rises again as n takes on larger values; this feature was observed also for the higher-dimensional Schwarzschild black hole [6] and, according to our results, persists also in the case of a Schwarzschild-de-Sitter background. As Λ ranges from 0.01 to 0.2,

for fixed n , the bulk-to-brane ratio is enhanced but by a moderate amount - we estimate that, for small values of n , by merely increasing the value of the cosmological constant we would not obtain a ratio larger than unity, and thus a bulk domination. The same seems to hold for small values of n and Λ in terms of the coupling ξ : a moderate enhancement appears as ξ changes from 0 to 1 (in fact, for $\xi = 1$, a slight decrease appears in the ratio as Λ increases, a feature that is probably attributed to the slightly more significant suppression of the bulk emission curves compared to the brane ones at the low-energy for this set of parameters).

As n increases, though, from $n = 2$ to $n = 4$ and finally to $n = 7$, the enhancement in terms of ξ becomes significant reaching a factor of order 3 or 4. This enhancement is again justified by the different suppression the effective mass has on the energy emission rates: for a brane scalar field the effective mass comes out to be larger than the one for a bulk scalar field by a factor of $\mathcal{O}(10)$, which then causes the significant suppression of the emission of the corresponding brane fields. The enhancement factor in terms of ξ , for the case $n = 7$, is now enough to raise the bulk-to-brane ratio to values larger than unity: for $\xi = 1$, the energy emitted in the bulk is 3 times larger than the one emitted on the brane. We expect that this ratio will take even larger values as ξ is increased further.

5 Conclusions

In this work, we have studied the problem of propagation of scalar fields in the gravitational background of a higher-dimensional Schwarzschild-de-Sitter black hole as well as on the projected-on-the-brane 4-dimensional background. The scalar fields were also assumed to have a non-minimal coupling to the corresponding, brane or bulk, scalar curvature that effectively acted as a mass term. Previous studies had addressed the topic of only minimally-coupled scalar fields in a higher-dimensional background [35, 36, 37] or non-minimally coupled fields in a 4-dimensional Schwarzschild-de-Sitter background [38]. A recent work of ours [39] had attacked the full problem but in an analytic way: that approach allowed us to derive analytic expressions for the bulk and brane scalar greybody factors and to study their properties; however, the validity of the approximate technique used relied on the assumption that both the cosmological constant and the non-minimal field coupling were small.

Here, we have returned to the same problem and performed a comprehensive study by deriving exact numerical results for propagation of non-minimally-coupled scalar fields both in the bulk and on the brane. We have dealt with each case separately, solved the corresponding equations of motion numerically in order to derive the radial part of the field and, in terms of the latter, determined the greybody factors, or transmission probabilities. The analytical solutions we had previously derived served as asymptotic boundary conditions as well as checking points for our numerical analysis. Both in the bulk and on the brane, we demonstrated that, as expected, there was a very good agreement between the analytic and numerical results at the low-energy regime, for small values of the cosmological constant and the non-minimal field coupling, while deviations started to appear as Λ , ξ or the energy of the emitted particle increased beyond the allowed regimes.

Our exact, numerical analysis allowed us to study in detail the behaviour of the greybody factors in terms of all the parameters of the model: the angular-momentum number l and non-minimal coupling ξ of the field, the cosmological constant Λ and number n of extra spacelike dimensions of spacetime. We have confirmed the suppression of the greybody factor, both for brane and bulk scalar fields, as either l or ξ increased. The same holds for the number of extra dimensions, while the dependence on the cosmological constant proved to be more subtle, exactly as our previous analytic study had hinted to: depending on the value of the non-minimal coupling constant, Λ can either help the emitted particle to overcome the gravitational barrier or suppresses its transmission probability.

Moving beyond the boundaries of our previous analytic work, and having at our disposal the exact greybody factors for arbitrary values of the parameters of the model, we then proceeded to calculate the differential energy emission rates for the Hawking radiation in the form of scalar fields by a higher-dimensional Schwarzschild-de-Sitter black hole both in the bulk and on the brane. The behaviour of the power spectra in terms of the parameters of the model was the result of the contributions of both the greybody factors and the black-hole temperature. Similarly for brane and bulk emission, the differential energy rates received non-negligible contributions only from the first six partial modes due to the spherical symmetry of the background. An increase in the number of extra dimensions, due to the significant enhancement of the black-hole temperature, resulted to the enhancement itself of the emission rate, both on the brane and in the bulk. The non-minimal coupling term of the scalar field with the – brane or bulk – scalar curvature acted as an effective mass term, as anticipated, with any increase in the value of the coupling ξ causing the suppression of the emission rates throughout the energy regime. The more subtle role of the cosmological constant was reflected also in the profile of the power spectra: for small values of ξ , the emission rate is enhanced at all frequencies, while as ξ increases the enhancement persists only at the high-energy regime and a simultaneous suppression appears at the lower part of the spectrum.

A conclusion that was also drawn from the above analysis was that the greybody factors for brane and bulk scalar fields exhibited differences in their profiles in terms of the parameters of the model; these differences appeared also in the corresponding energy emission rates. By computing the relative energy rates, we showed that, for small values of the cosmological constant and field coupling, the bulk channel was sub-dominant at the low and intermediate energy regime; as noted before, the bulk channel was significantly enhanced at the high-energy regime without surpassing though the brane channel. However, as the non-minimal field coupling, or equivalently the effective mass term, of the scalar fields increased, the bulk channel received an extra boost. When the above was combined also with a large number of extra spacelike dimensions, the bulk channel became the dominant one. The calculation of the exact ratio of bulk and brane emissivities showed that for $n = 7$ and $\xi = 1$ - a rather moderate value of the field coupling - the bulk channel emitted more energy per unit time by a factor of almost 4 compared to the brane channel. This has been one of the very few times (see also [19]) where the brane domination not only breaks down but, for a further increase of the field coupling, the brane emission could be only a very small part of the total output of energy from the Schwarzschild-de-Sitter black hole - and this has been caused by the addition

of a legitimate interaction term of the fields under study with the scalar curvature of spacetime.

Acknowledgements. T.P. would like to thank Dimitrios Karamitros for useful discussions. Part of this work was supported by the COST Action MP1210 “The String Theory Universe”.

References

- [1] N. Arkani-Hamed, S. Dimopoulos and G. R. Dvali, Phys. Lett. B **429**, 263 (1998); Phys. Rev. D **59**, 086004 (1999); I. Antoniadis, N. Arkani-Hamed, S. Dimopoulos and G. R. Dvali, Phys. Lett. B **436**, 257 (1998).
- [2] L. Randall and R. Sundrum, Phys. Rev. Lett. **83** (1999) 3370; Phys. Rev. Lett. **83** (1999) 4690.
- [3] F. Tangherlini, Nuovo Cim. **27** (1963) 636.
- [4] S. W. Hawking, Commun. Math. Phys. **43**, 199–220 (1975)
- [5] P. Kanti and J. March-Russell, Phys. Rev. D **66**, 024023 (2002); Phys. Rev. D **67**, 104019 (2003).
- [6] C. M. Harris and P. Kanti, JHEP **0310**, 014 (2003).
- [7] A. S. Cornell, W. Naylor and M. Sasaki, JHEP **0602**, 012 (2006); V. Cardoso, M. Cavaglia and L. Gualtieri, Phys. Rev. Lett. **96**, 071301 (2006); JHEP **0602**, 021 (2006); S. Creek, O. Efthimiou, P. Kanti and K. Tamvakis, Phys. Lett. B **635**, 39 (2006).
- [8] C. M. Harris and P. Kanti, Phys. Lett. B **633** (2006) 106; G. Duffy, C. Harris, P. Kanti and E. Winstanley, JHEP **0509**, 049 (2005).
- [9] M. Casals, P. Kanti and E. Winstanley, JHEP **0602**, 051 (2006).
- [10] M. Casals, S. Dolan, P. Kanti and E. Winstanley, JHEP **0703**, 019 (2007); JHEP **0806**, 071 (2008).
- [11] D. Ida, K. y. Oda and S. C. Park, Phys. Rev. D **67**, 064025 (2003) [Erratum-ibid. D **69**, 049901 (2004)]; Phys. Rev. D **71**, 124039 (2005); Phys. Rev. D **73**, 124022 (2006).
- [12] S. Creek, O. Efthimiou, P. Kanti and K. Tamvakis, Phys. Rev. D **75** (2007) 084043; Phys. Rev. D **76** (2007) 104013; Phys. Lett. B **656**, 102 (2007).
- [13] V. P. Frolov and D. Stojkovic, Phys. Rev. D **67**, 084004 (2003); H. Nomura, S. Yoshida, M. Tanabe and K. i. Maeda, Prog. Theor. Phys. **114**, 707 (2005); E. Jung and D. K. Park, Nucl. Phys. B **731**, 171 (2005); Mod. Phys. Lett. A **22**,

- 1635 (2007);
S. Chen, B. Wang, R. K. Su and W. Y. Hwang, JHEP **0803**, 019 (2008).
- [14] H. Kodama, Prog. Theor. Phys. Suppl. **172**, 11 (2008); Lect. Notes Phys. **769**, 427 (2009);
J. Doukas, H. T. Cho, A. S. Cornell and W. Naylor, Phys. Rev. D **80** (2009) 045021;
P. Kanti, H. Kodama, R. A. Konoplya, N. Pappas and A. Zhidenko, Phys. Rev. D **80** (2009) 084016.
- [15] A. Flachi, M. Sasaki and T. Tanaka, JHEP **0905** (2009) 031.
- [16] M. Casals, S. R. Dolan, P. Kanti and E. Winstanley, Phys. Lett. B **680** (2009) 365.
- [17] D. C. Dai and D. Stojkovic, JHEP **1008** (2010) 016.
- [18] M. O. P. Sampaio, JHEP **1203** (2012) 066.
- [19] J. Grain, A. Barrau and P. Kanti, Phys. Rev. D **72** (2005) 104016.
- [20] V. P. Frolov and D. Stojkovic, Phys. Rev. D **66**, 084002 (2002); Phys. Rev. Lett. **89**, 151302 (2002);
D. Stojkovic, Phys. Rev. Lett. **94**, 011603 (2005).
- [21] D. C. Dai, N. Kaloper, G. D. Starkman and D. Stojkovic, Phys. Rev. D **75**, 024043 (2007);
T. Kobayashi, M. Nozawa, Y. Takamizu, Phys. Rev. D **77**, 044022 (2008).
- [22] R. Jorge, E. S. de Oliveira and J. V. Rocha, Class. Quant. Grav. **32**, no. 6, 065008 (2015).
- [23] R. Dong and D. Stojkovic, Phys. Rev. D **92**, no. 8, 084045 (2015).
- [24] P. Kanti, Int. J. Mod. Phys. A **19**, 4899–4951 (2004).
- [25] G. L. Landsberg, Eur. Phys. J. C **33**, S927–S931 (2004).
- [26] A. S. Majumdar and N. Mukherjee, Int. J. Mod. Phys. D **14**, 1095–1129 (2005).
- [27] S. C. Park, Prog. Part. Nucl. Phys. **67**, 617–650 (2012).
- [28] B. Webber, eConf C **0507252**, T030 (2005) [hep-ph/0511128].
- [29] A. Casanova and E. Spallucci, Class. Quant. Grav. **23**, R45–R62 (2006).
- [30] P. Kanti, Lect. Notes Phys. **769**, 387–423 (2009).
- [31] P. Kanti, Rom. J. Phys. **57**, 879–893 (2012).
- [32] E. Winstanley, arXiv:0708.2656 [hep-th] (2007).
- [33] P. Kanti, J. Phys. Conf. Ser. **189**, 012020 (2009).

- [34] P. Kanti and E. Winstanley, arXiv:1402.3952 [hep-th].
- [35] P. Kanti, J. Grain and A. Barrau, Phys. Rev. D **71** (2005) 104002.
- [36] T. Harmark, J. Natario and R. Schiappa, Adv. Theor. Math. Phys. **14** (2010) 727.
- [37] S. F. Wu, S. y. Yin, G. H. Yang and P. M. Zhang, Phys. Rev. D **78**, 084010 (2008).
- [38] L. C. B. Crispino, A. Higuchi, E. S. Oliveira and J. V. Rocha, Phys. Rev. D **87** (2013) 10, 104034.
- [39] P. Kanti, T. Pappas and N. Pappas, Phys. Rev. D **90**, no. 12, 124077 (2014).
- [40] P. R. Anderson, A. Fabbri and R. Balbinot, Phys. Rev. D **91**, no. 6, 064061 (2015).
- [41] C. A. Sporea and A. Borowiec, Int. J. Mod. Phys. D **25**, no. 04, 1650043 (2016).
- [42] R. C. Myers and M. J. Perry, Annals Phys. **172**, 304 (1986).
- [43] C. Molina, Phys. Rev. D **68** (2003) 064007.
- [44] C. Muller, in *Lecture Notes in Mathematics: Spherical Harmonics* (Springer-Verlag, Berlin-Heidelberg, 1966).
- [45] D. N. Page, Phys. Rev. D **16** (1977) 2402.
- [46] E. I. Jung, S. H. Kim and D. K. Park, Phys. Lett. B **586** (2004) 390; JHEP **0409** (2004) 005; Phys. Lett. B **602** (2004) 105.
- [47] M. O. P. Sampaio, JHEP **0910** (2009) 008; JHEP **1002** (2010) 042.
- [48] P. Kanti and N. Pappas, Phys. Rev. D **82** (2010) 024039.
- [49] R. Bousso and S. W. Hawking, Phys. Rev. D **54**, 6312 (1996).
- [50] M. Bander and C. Itzykson, Rev. Mod. Phys. **38**, 330 (1966).